New Peak-to-Average Power-Ratio Reduction Algorithms for Multicarrier Communications

Y. J. Kou, W.-S. Lu, and A. Antoniou

Department of Electrical and Computer Engineering

University of Victoria

Victoria, B.C., V8W 3P6

Email: {ykou, wslu, aantoniou}@ece.uvic.ca

Abstract

New peak-to-average power-ratio reduction (PAPR) algorithms for multicarrier systems are deduced by applying joint optimization to the modulation constellation and the unused multicarrier subsymbols. For baseband multicarrier systems, a PAPR-reduction algorithm is developed using a fast linear programming approach where the exterior constellation points in active subchannels and subsymbols in unused subchannels are simultaneously optimized. It is shown that an optimal PAPR-reduction solution can be obtained using the proposed PAPR-reduction algorithm with high efficiency. For passband multicarrier systems where all subchannels are active, a new PAPR-reduction algorithm is established. Our simulations show that considerable performance improvement can be achieved by the proposed PAPR-reduction algorithm over several existing algorithms, and a tradeoff between performance and computational complexity can be obtained.

List of Figures

I. Introduction

Multicarrier modulation finds applications in both wired and wireless communications [1]-[5]. Well known examples of multicarrier modulation-based systems include digital subscriber lines (DSLs) using discrete multitone (DMT) [2], digital audio broadcasting (DAB) [3], and digital video broadcasting (DVB) [4] using orthogonal frequency-division multiplexing (OFDM).

A major problem of multicarrier modulation is its large peak-to-average power-ratio (PAPR), which makes system performance very sensitive to distortion introduced by nonlinear devices, e.g., power amplifiers (PAs). In order to mitigate nonlinear distortion, linear PAs with a wide dynamic range are required but such PAs are inefficient. A PA with high-power efficiency was developed in [6] based on an envelope elimination and restoration technique whereby the envelope and phase components of the multicarrier signal are treated separately. While the phase signal is fed directly into the PA, the envelope of the signal is used to modulate the power supply of the PA through a switch mode power supply. In this way, the efficiency of the PA is increased since it is largely independent of envelope fluctuations. However, the average output power would be low when large envelope fluctuations occur. In order to increase the average output power, clipping of the envelope signal would be needed but this operation would impair the bit-error rate (BER) performance of the system.

Another solution to the problem is to reduce the PAPR of the multicarrier signal before it enters the PA and recently a number of PAPR-reduction techniques and algorithms have been proposed. A straightforward way would be to limit the signal strength at the transmitter to a desired level but the technique degrades the BER performance of the system and, in addition, it increases the out-of-band radiation [7][8]. Methods that combine error-control coding with PAPR reduction were proposed in [9]-[11]. These methods reduce the data rate and are incompatible with

the existing standards. In [12][13], an approach was proposed that generates a set of multicarrier signals and selects the transmit signal with the lowest peak power. This method is computationally efficient but it requires transmission of side information. In [14], a new optimization criterion for partial transmit sequences to reduce PAPR is proposed. This technique also requires transmission of side information. The so-called tone reservation and tone injection methods were proposed in [15][16], respectively, for the reduction of the PAPR of the transmit signal. In the tone reservation method, several subcarriers are set aside for PAPR reduction. However, active subcarriers are not exploited for the reduction of the PAPR. In the tone injection method, the PAPR is reduced by forming a generalized constellation and selecting a proper mapping between the original and generalized constellation points. In [17], PAPR reduction is achieved by modifying the modulation constellation over active subcarriers in a way that will not degrade the BER performance. This method does not guarantee an optimal PAPR-reduction solution.

In this paper, PAPR-reduction algorithms that offer improved performance are proposed. First, the *feasible region* of the modulation constellation point is identified. New PAPR-reduction algorithms for baseband and passband multicarrier systems are then deduced by modifying the modulation constellation over active subcarriers and the modulation symbols over unused subcarriers. Using the proposed PAPR-reduction algorithms, optimal PAPR-reduction solutions can be obtained and for baseband multicarrier systems, considerable performance improvement can be achieved over that achieved with the algorithms in [15][17]. For passband multicarrier systems where all subcarriers are active, a new PAPR-reduction algorithm is constructed whereby the associated minimax optimization problem is solved using an accelerated *least-pth* algorithm [18]. Simulation results are presented which demonstrate that the proposed method outperforms the method in [17] and that improved PAPR reduction can be obtained when the method of [13] is

combined with the method proposed in this paper.

The paper is organized as follows. The multicarrier system model is described in Sec. II. After a brief review of the existing PAPR reduction methods reported in [15][17] in Sec. III, the proposed PAPR-reduction algorithms are developed in Sec. IV for the baseband case and in Sec. V for the passband case. Then, simulation results are presented in Sec. VI. Conclusions are drawn in Sec. VII.

II. System Description and Problem Formulation

Consider a typical multicarrier transmitter as illustrated in Fig. 1, where the blocks S/P, P/S, and D/A represent serial-to-parallel interface, parallel-to-serial interface, and digital-to-analog converter, respectively, and Amp. represents a power amplifier. The available bandwidth B in the system is divided into N *subchannels* whose center frequencies are seperated by B/N. Each of the subchannels is independently modulated using phase-shift keying (PSK) or quadrature amplitude modulation (QAM). The modulated symbol X_k is referred to as the *subsymbol* in the kth subchannel [2], and vector $\mathbf{X} = [X_1, \ldots, X_N]^T$ is referred to as the multicarrier symbol.

Fig. 1. A multicarrier transmitter.

The multicarrier transmit signal $\mathbf{x}$ can be obtained using the inverse discrete Fourier transform (IDFT) as

$$x_n = \frac{1}{N} \sum_{k=1}^{N} X_k e^{j2\pi(k-1)(n-1)/N} \quad \text{for } k = 1, \ldots, N \tag{1}$$

where x_n and X_n represent the nth elements of vectors $\mathbf{x}$ and $\mathbf{X}$, respectively. In matrix form, (1)

can be expressed as

$$\mathbf{x} = \mathbf{Q}\mathbf{X} \tag{2}$$

where $\mathbf{Q}$ is the IDFT matrix with elements $q_{n,k} = (1/N)e^{j2\pi(k-1)(n-1)/N}$ for $n,\ k = 1, 2, \ldots, N$. In a baseband transmission system, $\mathbf{x}$ has to be real, and, therefore, the input signal to the IDFT processor must meet the conjugate symmetric conditions [2]. On the other hand, $\mathbf{x}$ can be a complex signal in a passband transmission system. With this difference noted, the block diagram in Fig. 1 applies to both baseband and paseband transmitters.

For the multicarrier system in Fig. 1, the PAPR of signal $\mathbf{x}$ is defined as

$$\text{PAPR}_0 = \frac{\|\mathbf{x}\|_\infty^2}{\mathcal{E}[\|\mathbf{x}\|_2^2]/N} \tag{3}$$

where $\mathcal{E}[\cdot]$ denotes expectation, and $\|\mathbf{x}\|_\infty$ and $\|\mathbf{x}\|_2$ represent the infinity- and 2-norm of vector $\mathbf{x}$, respectively.

The PAPR of the multicarrier signal can be minimized without BER degradation if the time-domain signal $\mathbf{x}$ (equivalently, the frequency-domain signal $\mathbf{X}$) is appropriately modified. Analytically, one seeks to find a vector $\mathbf{c}$ (equivalently, vector $\mathbf{C}$) that modifies $\mathbf{x}$ to $\mathbf{x}+\mathbf{c}$ (equivalently, $\mathbf{X}$ to $\mathbf{X}+\mathbf{C}$) such that the PAPR for the modified signal, i.e.,

$$\text{PAPR}\,(\mathbf{c}) = \frac{\|\mathbf{x}+\mathbf{c}\|_\infty^2}{\mathcal{E}[\|\mathbf{x}\|_2^2]/N} \tag{4}$$

is minimized such that the BER performance is not degraded. The above definition was adopted in [15] and has since been used by a number of authors [16][19][20]. Note that vectors $\mathbf{c}$ and $\mathbf{C}$ are related to each other by

$$\mathbf{x}+\mathbf{c} = \mathbf{Q}\,(\mathbf{X}+\mathbf{C})\,. \tag{5}$$

It follows from (2) and (5) that

$$\mathbf{c} = \mathbf{Q}\mathbf{C}. \tag{6}$$

In the rest of the paper, vectors $\mathbf{c}$ and $\mathbf{C}$ in (6) will be referred to as the time-domain and frequency-domain *peak-reduction vectors*, respectively.

III. Review of Previous Work

A. LP-based method for baseband transmission

It follows from Eqs. (3)-(6) that for a given signal $\mathbf{x}$, the vector $\mathbf{c}$ that minimizes PAPR($\mathbf{c}$) is the solution of the optimization problem

$$\underset{\mathbf{c}}{\text{minimize}} \ \|\mathbf{x}+\mathbf{c}\|_\infty = \ \underset{\mathbf{C}}{\text{minimize}} \ \|\mathbf{x}+\mathbf{QC}\|_\infty. \tag{7}$$

In the methods proposed in [15], the transmitter and the receiver reserve a small subset of subchannels for generating the peak-reduction vector so that the BER performance of the system is not decreased. Analytically, this means that if there are n_u unused subchannels whose indices form the set $\mathcal{I}_u = \{j_1, j_2, \ldots, j_{n_u}\}$, then the components X_k for $k \in \mathcal{I}_u$ are set to zero and the components C_k are nonzero only if $k \in \mathcal{I}_u$. Therefore, the optimization problem can be formulated as

$$\underset{\mathbf{C}}{\text{minimize}} \|\mathbf{x}+\mathbf{QC}\|_\infty \tag{8a}$$

$$\text{subject to:} \quad C_k = 0 \ for \ k \notin \mathcal{I}_u. \tag{8b}$$

Let $\hat{\mathbf{C}} = [C_{j_1} \ C_{j_2} \ \cdots \ C_{j_{n_u}}]^T$ and $\hat{\mathbf{Q}} = [\mathbf{q}_{j_1} \ \mathbf{q}_{j_2} \ \cdots \ \mathbf{q}_{j_{n_u}}]$ where $\mathbf{q}_{j_k}$ is the j_kth column of $\mathbf{Q}$. If $\mathbf{c} = \mathbf{QC} = \hat{\mathbf{Q}}\hat{\mathbf{C}}$, the problem in (8) can be converted to the problem

$$\underset{\hat{\mathbf{C}}}{\text{minimize}} \ \|\mathbf{x}+\hat{\mathbf{Q}}\hat{\mathbf{C}}\|_\infty \tag{9}$$

where the dimension of vector $\hat{\mathbf{C}}$ is n_u. It can be shown that the above problem can be cast as a linear programming (LP) problem with $2n_u + 1$ variables [15][16].

B. Method for baseband transmission

In the method of [17], it is assumed that all subchannels are active and the peak-reduction vector $\mathbf{C}$ is generated through a reassignment of the constellation points as illustrated below. Let us consider a specific case of OFDM with quadrature phase-shift keying (QPSK) modulation in each subchannel. As shown in Fig. 2, the conventional QPSK constellation points are located at the corners of the shaded regions. Each of these regions is called a *feasible region* for the reason that if a conventional constellation point is reassigned to a point inside the corresponding shaded region, the BER performance will not be degraded because the minimum distance between the newly assigned constellaton point and any constellation point located in other feasible regions is guaranteed not to be less than the minimum distance among the conventional constellation points. In the rest of the paper, a constellation point is said to be *feasible* if it is located within the associated feasible region.

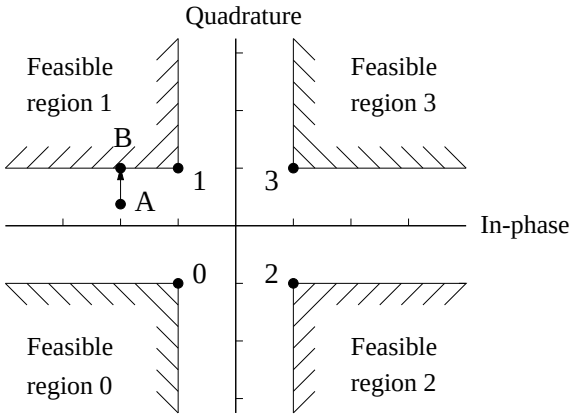

Fig. 2. Modification of a QPSK constellation point in an active subchannel.

Let $\mathbf{X}^{(0)}$ be the original multicarrier symbol obtained using QPSK modulation of a given data stream. The time-domain signal $\mathbf{x}^{(0)}$ is obtained as the IDFT of $\mathbf{X}^{(\mathbf{0})}$. For the components of $\mathbf{x}^{(0)}$ whose magnitudes exceed a certain target peak level, a clipping operation is used to limit

their magnitudes to the target peak level. Denoting the modified time-domain signal by $\mathbf{x}^{(1)}$, we perform the DFT of $\mathbf{x}^{(1)}$ to obtain the multicarrier symbol $\mathbf{X}^{(1)}$. Due to the clipping operation, some subsymbols of $\mathbf{X}^{(1)}$ may lie outside their feasible regions. In order to avoid BER degradation, these subsymbols need to be modified properly. Suppose subsymbol $X_k^{(0)}$ is at corner point 1 as illustrated in Fig. 2, which becomes $X_k^{(1)}$ at point A after the application of IDFT, clipping, and DFT. Denoting the point that is feasible and nearest to point A as B, we modify $X_k^{(1)}$ such that it is represented by point B. If necessary, this IDFT/clipping/DFT/reassignment procedure is repeated for another $K-1$ times until the maximum magnitude of $\mathbf{x}^{(K)}$ is not larger than the target peak value.

IV. PAPR Reduction for Baseband Multicarrier Systems

A. System and modulation schemes

We consider an N-subchannel baseband multicarrier system with a modulation scheme that can be either QPSK or 16-QAM [15]-[17] and assume that the system has a certain number of unused subchannels. The number and index set of unused subchannels are denoted as n_u and $\mathcal{I}_u = \{j_1, j_2, \ldots, j_{n_u}\}$, respectively. The number and index set of active subchannels that are chosen for PAPR-reduction are denoted as n_a and $\mathcal{I}_a = \{i_1, i_2, \ldots, i_{n_a}\}$, respectively. The index numbers are arranged such that $i_1 < i_2 < \cdots < i_{n_a}$ and $j_1 < j_2 < \cdots < j_{n_u}$ and sets $\mathcal{I}_a$ and $\mathcal{I}_u$ do not intersect. In the subsequent development, the concept of feasible region will be frequently used and it needs to be clarified first. For QPSK modulation, the feasible region was defined in Sec. III (see Fig. 2). For 16-QAM modulation, the feasible regions are shown in Fig. 3. As can be seen, for each of the interior constellation points (i.e., points 5, 7, 13, 15), the feasible region is reduced to the point itself, meaning that the interior constellation point is not allowed to change.

For each of the exterior constellation points at the corners (i.e., points 0, 2, 8, 10), the feasible region is the corresponding shaded region. For each of the non-corner exterior constellation points (i.e., points 1, 3, 4, 6, 9, 11, 12, 14), the feasible region is a line which starts at the constellation point and extends to infinity.

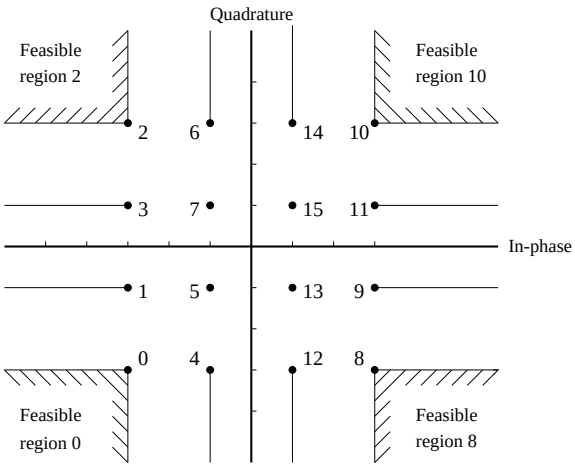

Fig. 3. Feasible region for 16-QAM constellation points.

B. Algorithm

In the proposed method, the peak-reduction vector $\mathbf{C}$ is modified in the selected subchannels whose index falls into either $\mathcal{I}_u$ or $\mathcal{I}_a$ so as to minimize $\|\mathbf{x} + \mathbf{QC}\|_\infty$ such that the modified subsymbols in the active subchannels remain feasible. Obviously, this is a constrained optimization problem which can be formulated as

$$\underset{\mathbf{C}}{\text{minimize}} \quad \|\mathbf{x} + \mathbf{QC}\|_\infty \tag{10a}$$

$$\text{subject to: } X_k + C_k \text{ feasible for } k \in \mathcal{I}_a \tag{10b}$$

$$C_k = 0 \text{ for } k \notin \mathcal{I}_u \text{ and } k \notin \mathcal{I}_a. \tag{10c}$$

It is worthwhile to note that by allowing point $X_k + C_k$ ($k \in \mathcal{I}_a$) to move within the feasible region, a solution of (10) can be obtained which is expected to outperform that of (8).

If we denote $\tilde{\mathbf{C}}$ as the subvector of $\mathbf{C}$ that is composed of the elements with indices in $\mathcal{I}_u$ and $\mathcal{I}_a$, and denote $\tilde{\mathbf{Q}}$ as the submatrix of $\mathbf{Q}$ that is composed of the columns with indices in $\mathcal{I}_u$ and $\mathcal{I}_a$, then the problem in (10) can be converted to

$$\underset{\tilde{\mathbf{C}}}{\text{minimize}} \quad \|\mathbf{x} + \tilde{\mathbf{Q}}\tilde{\mathbf{C}}\|_\infty \tag{11a}$$

$$\text{subject to: } X_k + C_k \text{ feasible for } k \in \mathcal{I}_a. \tag{11b}$$

Let τ be the upper bound of the objective function in (11a). It can be readily shown that by including parameter τ as an additional design variable, the constrainted optimization problem in (11) can be formulated as

$$\text{minimize} \quad \tau \tag{12a}$$

$$\text{subject to: } |x_k + \tilde{\mathbf{q}}_k^T \tilde{\mathbf{C}}| \le \tau \quad \text{for } k = 1, \ldots, N \tag{12b}$$

$$X_k + C_k \text{ feasible} \quad \text{for } k \in \mathcal{I}_a \tag{12c}$$

where $\tilde{\mathbf{q}}_k^T$ denotes the kth row of $\tilde{\mathbf{Q}}$. Note that in general matrix $\tilde{\mathbf{Q}}$ and vector $\tilde{\mathbf{C}}$ are complex valued. If we let $\tilde{\mathbf{Q}} = \tilde{\mathbf{Q}}_r + j\tilde{\mathbf{Q}}_i$ and $\tilde{\mathbf{C}} = \tilde{\mathbf{C}}_r + j\tilde{\mathbf{C}}_i$, then the constraints in (12b) can be expressed in matrix form as

$$\begin{bmatrix} -\tilde{\mathbf{Q}}_r & \tilde{\mathbf{Q}}_i & \mathbf{e} \\ \tilde{\mathbf{Q}}_r & -\tilde{\mathbf{Q}}_i & \mathbf{e} \end{bmatrix} \begin{bmatrix} \tilde{\mathbf{C}}_r \\ \tilde{\mathbf{C}}_i \\ \tau \end{bmatrix} \ge \begin{bmatrix} -\mathbf{x} \\ \mathbf{x} \end{bmatrix} \tag{13}$$

where $\mathbf{e} = [1\ 1\ \cdots\ 1]^T \in \mathcal{R}^{N\times 1}$, and the optimization problem in (12) becomes

$$\text{minimize} \quad \tau \tag{14a}$$

$$\text{subject to:} \quad \begin{bmatrix} -\tilde{\mathbf{Q}}_r & \tilde{\mathbf{Q}}_i & \mathbf{e} \\ \tilde{\mathbf{Q}}_r & -\tilde{\mathbf{Q}}_i & \mathbf{e} \end{bmatrix} \begin{bmatrix} \tilde{\mathbf{C}}_r \\ \tilde{\mathbf{C}}_i \\ \tau \end{bmatrix} \ge \begin{bmatrix} -\mathbf{x} \\ \mathbf{x} \end{bmatrix} \tag{14b}$$

$$X_k + C_k \text{ feasible} \quad \text{for } k \in \mathcal{I}_a. \tag{14c}$$

In what follows, we further convert the problem in (14) into an explicit linear programming (LP) problem for different modulation schemes.

B.1 QPSK Modulation Case

For QPSK modulation, all constellation points are exterior points and each is associated with a large feasible region, as shown in Fig. 2. By defining vectors $\mathbf{d} = [0 \cdots 0\ 1]^T \in \mathcal{R}^{2(n_u+n_a)+1}$ and $\mathbf{y} = [\tilde{\mathbf{C}}_r^T\ \tilde{\mathbf{C}}_i^T\ \tau]^T$, the objective function in (14a) becomes $\mathbf{d}^T\mathbf{y}$ and the constraints in (14b) become

$$\begin{bmatrix} -\tilde{\mathbf{Q}}_r & \tilde{\mathbf{Q}}_i & \mathbf{e} \\ \tilde{\mathbf{Q}}_r & -\tilde{\mathbf{Q}}_i & \mathbf{e} \end{bmatrix} \mathbf{y} \geq \begin{bmatrix} -\mathbf{x} \\ \mathbf{x} \end{bmatrix}. \tag{15}$$

If we denote $\tilde{\mathbf{X}}$ as a subvector of $\mathbf{X}$ composed of the elements with indices in $\mathcal{I}_u$ or $\mathcal{I}_a$, then the constraints in (14c) can be expressed as

$$S_{rk}C_{rk} \geq 0 \quad \text{for } k \in \mathcal{I}_a \tag{16a}$$

$$S_{ik}C_{ik} \geq 0 \quad \text{for } k \in \mathcal{I}_a \tag{16b}$$

where $S_{rk} = \text{sgn}[\text{real}(X_k)]$, $S_{ik} = \text{sgn}[\text{imag}(X_k)]$, $C_{rk} = \text{real}(C_k)$, and $C_{ik} = \text{imag}(C_k)$. The constraints in (16) can be put together in matrix form as

$$\begin{bmatrix} \mathbf{S}_r & \mathbf{0} & \mathbf{0} \\ \mathbf{0} & \mathbf{S}_i & \mathbf{0} \end{bmatrix} \mathbf{y} \geq \begin{bmatrix} \mathbf{0} \\ \mathbf{0} \end{bmatrix} \tag{17}$$

where $\mathbf{S}_r$ and $\mathbf{S}_i$ are $n_a \times N$ matrices that can be generated by filling the $(k, i_k)th$ component of the zero matrix of the same size with S_{rk} and S_{ik}, respectively, for $k = 1,\ 2,\ \ldots,\ n_u$. Furthermore, the linear constraints in (15) and (17) can be combined and the optimization problem at hand can be formulated as

$$\text{minimize} \quad \mathbf{d}^T\mathbf{y} \tag{18a}$$

$$\text{subject to:} \quad \mathbf{A}\mathbf{y} \geq \mathbf{b} \tag{18b}$$

with

$$\mathbf{A} = \begin{bmatrix} -\tilde{\mathbf{Q}}_r & \tilde{\mathbf{Q}}_i & \mathbf{e} \\ \tilde{\mathbf{Q}}_r & -\tilde{\mathbf{Q}}_i & \mathbf{e} \\ \mathbf{S}_r & \mathbf{0} & \mathbf{0} \\ \mathbf{0} & \mathbf{S}_i & \mathbf{0} \end{bmatrix}, \quad \mathbf{b} = \begin{bmatrix} -\mathbf{x} \\ \mathbf{x} \\ \mathbf{0} \\ \mathbf{0} \end{bmatrix}. \tag{18c}$$

The problem in (18) is an LP problem with $2(n_a+n_u)+1$ variables and $2N+2n_a$ constraints. Since N $> n_u$, the number of constraints in (18) is always greater than the number of the design variables This LP problem can be sovled by a recently proposed Newton method [21] which works more efficiently relative to standard solution methods for LP problems, especially when the number of constraints is considerably greater than the number of design variables.

B.2 16-QAM Modulation Case

In the QPSK modulation case, all constellation points are exterior points. In contrast, in the 16-QAM modulation case, there are four interior constellation points $\mathcal{G}_0 = \{5,\ 7,\ 13,\ 15\}$ that are fixed, eight constellation points $\mathcal{G}_1 = \{1,\ 3,\ 4,\ 6,\ 9,\ 11,\ 12,\ 14\}$ with each allowed to move along a line, and four constellation points $\mathcal{G}_2 = \{0,\ 2,\ 8,\ 10\}$ at corners. Consequently, the constraints in (14b) and (14c) have to be handled by distinguishing these sets of points.

For each selected active subchannel k ($k \in \mathcal{I}_a$), if the modulated subsymbol X_k belongs to index set $\mathcal{G}_0$, then the corresponding C_k is set to zero; if X_k belongs to $\mathcal{G}_2$, then C_k is constrained exactly in the same way as in the QPSK case; if X_k belongs to $\mathcal{G}_1$, then we have to further distinguish the possible cases: if X_k belongs to set $\mathcal{G}_{11} = \{1,\ 3,\ 9,\ 11\}$, then the *imaginary* component of C_k is set to zero; if X_k belongs to $\mathcal{G}_{12} = \{4,\ 6,\ 12,\ 14\}$, then the *real* component of C_k is set to zero. Accordingly, three index sets, denoted as $\mathcal{I}_{a11}$, $\mathcal{I}_{a12}$, and $\mathcal{I}_{a2}$, can be defined as follows. An index k ($k \in \mathcal{I}_a$) belongs to set $\mathcal{I}_{a11}$ or $\mathcal{I}_{a12}$ or $\mathcal{I}_{a2}$, if the constellation point associated with subsymbol

X_k belongs to $\mathcal{G}_{a11}$ or $\mathcal{G}_{a12}$ or $\mathcal{G}_{a2}$, respectively.

In order to formulate the optimization problem properly, the following notation will be used:

- The submatrices of matrix $\mathbf{Q}$ composed of the columns with indices in $\mathcal{I}_u$, $\mathcal{I}_{a11}$, $\mathcal{I}_{a12}$, and $\mathcal{I}_{a2}$ will be denoted as $\mathbf{Q}_u$, $\mathbf{Q}_{a11}$, $\mathbf{Q}_{a12}$, and $\mathbf{Q}_{a2}$, respectively.
- The subvectors of $\mathbf{C}$ composed of the elements with indices in $\mathcal{I}_u$, $\mathcal{I}_{a11}$, $\mathcal{I}_{a12}$, and $\mathcal{I}_{a2}$ will be denoted as $\mathbf{C}_u$, $\mathbf{C}_{a11}$, $\mathbf{C}_{a12}$, and $\mathbf{C}_{a2}$, respectively. The subvectors $\mathbf{X}_u$, $\mathbf{X}_{a11}$, $\mathbf{X}_{a12}$, and $\mathbf{X}_{a2}$ of vector $\mathbf{X}$ are defined similarly.
- The real and imaginary parts of matrix $\mathbf{Q}_u$ will be denoted as $\mathbf{Q}_{r,u}$ and $\mathbf{Q}_{i,u}$, respectively. The real and imaginary parts of vector $\mathbf{C}_u$ will be denoted as $\mathbf{C}_{r,u}$ and $\mathbf{C}_{i,u}$, respectively.
- Diagonal matrices $\mathbf{S}_{r,a11}$ and $\mathbf{S}_{i,a11}$, etc. will be represented by $\mathbf{S}_{r,a11} = \mathrm{diag}[\mathrm{sgn}(\mathbf{X}_{r,a11})]$ and $\mathbf{S}_{i,a11} = \mathrm{diag}[\mathrm{sgn}(\mathbf{X}_{i,a11})]$, etc.

The optimization problem in (14) can now be formulated more explicitly as

$$\text{minimize} \quad \hat{\mathbf{d}}^T \hat{\mathbf{y}} \tag{19a}$$

$$\text{subject to:} \quad \hat{\mathbf{A}}\hat{\mathbf{y}} \geq \hat{\mathbf{b}}. \tag{19b}$$

where

$$\hat{\mathbf{d}} = \begin{bmatrix} 0 \\ \vdots \\ 0 \\ 1 \end{bmatrix}, \qquad \hat{\mathbf{y}} = \begin{bmatrix} \hat{\mathbf{C}}_r \\ \hat{\mathbf{C}}_i \\ \tau \end{bmatrix}, \qquad \hat{\mathbf{A}} = \begin{bmatrix} -\hat{\mathbf{Q}}_r & \hat{\mathbf{Q}}_i & \mathbf{e} \\ \hat{\mathbf{Q}}_r & -\hat{\mathbf{Q}}_i & \mathbf{e} \\ \hat{\mathbf{S}}_r & \mathbf{0} & \mathbf{0} \\ \mathbf{0} & \hat{\mathbf{S}}_i & \mathbf{0} \end{bmatrix}, \quad \hat{\mathbf{b}} = \begin{bmatrix} \mathbf{x} \\ \mathbf{x} \\ \mathbf{0} \\ \mathbf{0} \end{bmatrix}, \quad \hat{\mathbf{e}} = \begin{bmatrix} 1 \\ \vdots \\ 1 \\ 1 \end{bmatrix},$$

$$\hat{\mathbf{C}}_r = \begin{bmatrix} \mathbf{C}_{r,u} \\ \mathbf{C}_{r,a2} \\ \mathbf{C}_{r,a11} \end{bmatrix}, \hat{\mathbf{C}}_i = \begin{bmatrix} \mathbf{C}_{i,u} \\ \mathbf{C}_{i,a2} \\ \mathbf{C}_{i,a12} \end{bmatrix}, \hat{\mathbf{S}}_r = \begin{bmatrix} \mathbf{0} & \mathbf{S}_{r,a2} & \mathbf{0} \\ \mathbf{0} & \mathbf{0} & \mathbf{S}_{r,a11} \end{bmatrix}, \hat{\mathbf{S}}_i = \begin{bmatrix} \mathbf{0} & \mathbf{S}_{i,a2} & \mathbf{0} \\ \mathbf{0} & \mathbf{0} & \mathbf{S}_{i,a12} \end{bmatrix},$$

$$\hat{\mathbf{Q}}_r = [\, \mathbf{Q}_{r,u} \quad \mathbf{Q}_{r,a2} \quad \mathbf{Q}_{r,a11} \,], \text{ and } \hat{\mathbf{Q}}_i = [\, \mathbf{Q}_{i,u} \quad \mathbf{Q}_{i,a2} \quad \mathbf{Q}_{i,a12} \,]. \tag{19c}$$

The problem in (19) is an LP problem with $1+n_{a11}+n_{a12}+2(n_{a2}+n_u)$ variables and $n_{a11}+n_{a12}+2(n_{a2}+n_u+N)$ constraints, where n_{a11}, n_{a12}, n_{a2} denote the sizes of index sets $\mathcal{I}_{a11}$, $\mathcal{I}_{a12}$, $\mathcal{I}_{a2}$, respectively.

On comparing the LP problem in (18) with that in (19), we see that the structures of the objective function as well as the constraints in (19) have been preserved.

B.3 Other Modulation Cases

For other modulation schemes such as K-QAM with K $>$ 16, feasible regions similiar to that in Fig. 3 can be defined and, with straightforward modification of the data set $\{\hat{\mathbf{A}}, \hat{\mathbf{y}}, \hat{\mathbf{b}}\}$ (see (19)), the corresponding PAPR-reduction problem can be formulated as standard LP problem. We conclude this section with two remarks.

Remark 1: In the proposed PAPR-redcution algorithm, the number of active subchannels involved in the optimization can vary. Therefore, the algorithm offers a certain degree of flexibility between computational complexity and performance. For example, maximum PAPR-reduction performance can be achieved at the cost of increased computational complexity if the proposed algorithm is applied to all of the active subchannels, (i.e., $n_a = \mathrm{N} - n_u$). On the other hand, if the algorithm is applied to a reduced number of active subchannels, then it becomes computationally more efficient at the cost of performance degradation.

Remark 2: For the sake of simplicity, only the Nyquist sampling rate is considered in the derivation of the above algorithm. However, with straightforward modifications the algorithm can be extended to systems where the time-domain signals are oversampled.

V. PAPR Rreduction for Passband Multicarrier Systems

A. System and modulation schemes

We consider an N-subchannel passband multicarrier system with a modulation scheme that can be either QPSK or 16-QAM [15]-[17]. In order to guarantee maximum data transmission rate, we assume that there are no unused subchannels in the system. The number and index set of active subchannels that are chosen for PAPR-reduction are denoted as n_a and $\mathcal{I}_u = \{j_1, j_2, \ldots, j_{n_a}\}$, respectively.

B. Algorithm

In the proposed method, the peak-reduction vector $\mathbf{C}$ is modified in selected active subchannels so as to minimize $\|\mathbf{x} + \mathbf{QC}\|_\infty$ subject to the modified subsymbols in the active subchannels remaining feasible. Denote $\tilde{\mathbf{C}}$ as the subvector of $\mathbf{C}$ composed of the elements with indices in $\mathcal{I}_a$. Denote $\tilde{\mathbf{Q}}$ as the submatrix of $\mathbf{Q}$ composed of columns with indices in $\mathcal{I}_a$. Such problem can be formulated as

$$\underset{\tilde{\mathbf{C}}}{\text{minimize}} \quad \|\mathbf{x} + \tilde{\mathbf{Q}}\tilde{\mathbf{C}}\|_\infty \tag{20a}$$

$$\text{subject to: } X_k + C_k \text{ feasible for } k \in \mathcal{I}_a. \tag{20b}$$

If we denote the kth row of $\tilde{\mathbf{Q}}$ as $\tilde{\mathbf{q}}_k^T$ and kth component of $\mathbf{x}$ by x_k , then the objective function in (20a) is the infinity norm of an N-dimensional vector whose kth component is $x_k + \tilde{\mathbf{q}}_k^T\tilde{\mathbf{C}}$, and the problem in (20) can be formulated as the *minimax* problem

$$\underset{\tilde{\mathbf{C}}}{\text{minimize}} \ \underset{1\le k\le N}{\text{maximize}} \quad \|x_k + \tilde{\mathbf{q}}_k^T\tilde{\mathbf{C}}\| \tag{21a}$$

$$\text{subject to: } X_k + C_k \text{ feasible} \quad \text{for } k \in \mathcal{I}_a \tag{21b}$$

Note that in general x_k and vectors $\tilde{\mathbf{q}}_k^T$ and $\tilde{\mathbf{C}}$ are complex valued. If we let $x_k = x_{r,k} + jx_{i,k}$,

$\tilde{\mathbf{q}}_k = \tilde{\mathbf{q}}_{r,k} + j\tilde{\mathbf{q}}_{i,k}$ and $\tilde{\mathbf{C}} = \tilde{\mathbf{C}}_r + j\tilde{\mathbf{C}}_i$, then the norm in (21a) assumes the form

$$\|\hat{\mathbf{x}}_k + \mathbf{P}_k\hat{\mathbf{C}}\| \tag{22a}$$

where

$$\hat{\mathbf{x}}_k = \begin{bmatrix} x_{r,k} \\ \\ x_{i,k} \end{bmatrix}, \ \mathbf{P}_k = \begin{bmatrix} \tilde{\mathbf{q}}_{r,k}^T & -\tilde{\mathbf{q}}_{i,k}^T \\ \\ \tilde{\mathbf{q}}_{i,k}^T & \tilde{\mathbf{q}}_{r,k}^T \end{bmatrix}, \ \hat{\mathbf{C}} = \begin{bmatrix} \tilde{\mathbf{C}}_r \\ \\ \tilde{\mathbf{C}}_i \end{bmatrix}. \tag{22b}$$

and the problem in (21) can be expressed as

$$\underset{\hat{\mathbf{C}}}{\text{minimize}} \ \underset{1\le k\le N}{\text{maximize}} \quad \|\hat{\mathbf{x}}_k + \mathbf{P}_k\hat{\mathbf{C}}\| \tag{23a}$$

$$\text{subject to:} \ \ X_k + C_k \text{ feasible} \quad \text{for } k \in \mathcal{I}_a \tag{23b}$$

In what follows we show that for several important mudulation schemes, the problem in (23) can be converted to an unconstrained optimization problem.

B.1 QPSK Modulation Case

As in the baseband case, the constraints in (23) can be formulated as the inequalities in (16). Essentially, these constraints require that the signs of C_{rk} and C_{ik} be identical to those of S_{rk} and S_{ik}, respectively. If we define a sign vector $\mathbf{s}$ as

$$\mathbf{s} = [\, s_1 \ \cdots \ s_{n_a} \ \ s_{n_a+1} \ \cdots \ s_{2n_a} \,]^T = [\, S_{r1} \ \cdots \ S_{rn_a} \ \ S_{i1} \ \cdots \ S_{in_a} \,]^T \tag{24}$$

then the constraints in (23b) can be eliminated by assuming vector $\hat{\mathbf{C}}$ to be of the form

$$\hat{\mathbf{C}} = [\, s_1 y_1^2 \ \cdots \ s_{n_a} y_{n_a}^2 \ \ s_{n_a+1} y_{n_a+1}^2 \ \cdots \ s_{2n_a} y_{2n_a}^2 \,]^T. \tag{25}$$

where y_i is the ith component of an unconstrained parameter vector $\mathbf{y} = [y_1 \cdots y_{2n_a}]^T$, and the problem in (23) is converted to

$$\underset{\mathbf{y}}{\text{minimize}} \ \underset{1\le k\le N}{\text{maximize}} \quad \|\hat{\mathbf{x}}_k + \hat{\mathbf{P}}_k\mathbf{y}^2\| \tag{26}$$

where $\hat{\mathbf{P}}_k$ is obtained by multiplying each column of $\mathbf{P}_k$ by the corresponding component of vector $\mathbf{s}$, and $\mathbf{y}^2$ denotes the vector obtained by squaring the components of vector $\mathbf{y}$. Efficient optimization algorithms are available in the literature that can be used to solve the minimax problem in (26), see, for example, [20], where an accelerated *least-pth* approach is proposed for minimax optimization.

B.2 16-QAM Modulation Case

In the 16-QAM modulation case, the sign vector in (24) needs to be modified to

$$\begin{aligned} \mathbf{s} &= [\,\hat{s}_1 \quad \cdots \quad \hat{s}_{n_{a11}+n_{a2}} \quad \hat{s}_{n_{a11}+n_{a2}+1} \quad \cdots \quad \hat{s}_{n_{a11}+n_{a12}+2n_{a2}}\,]^T \\ &= [\,\hat{S}_{r1} \quad \cdots \quad \hat{S}_{rn_{a11}+n_{a2}} \quad \hat{S}_{i1} \quad \cdots \quad \hat{S}_{in_{a12}+n_{a2}}\,]^T \end{aligned} \tag{27}$$

where $\hat{S}_{ri}$ and $\hat{S}_{ii}$ are the ith diagonal elements of $\hat{\mathbf{S}}_r$ and $\hat{\mathbf{S}}_i$ in (19c), respectively, and vector $\hat{\mathbf{C}}$ in (23) assumes the form

$$\hat{\mathbf{C}} = [\,\hat{s}_1 y_1^2 \cdots \hat{s}_{n_{a11}+n_{a2}} y^2_{n_{a11}+n_{a2}} \quad \hat{s}_{n_{a11}+n_{a2}+1} y^2_{n_{a11}+n_{a2}+1} \cdots \hat{s}_{n_{a11}+n_{a12}+2n_{a2}} y^2_{n_{a11}+n_{a12}+2n_{a2}}\,]^T. \tag{28}$$

Under these circumstances, the constraints in (23b) are eliminated and the problem in (23) is converted to

$$\underset{\tilde{\mathbf{y}}}{\text{minimize}} \;\; \underset{1\le k\le N}{\text{maximize}} \quad \|\hat{\mathbf{x}}_k + \hat{\mathbf{R}}_k \mathbf{y}^2\| \tag{29}$$

where $\mathbf{y} = [y_1 \cdots y_{n_{a11}+n_{a12}+2n_{a2}}]^T$ and $\hat{\mathbf{R}}_k$ is obtained by multiplying each column of $\mathbf{P}_k$ by the corresponding component of vector $\hat{\mathbf{s}}$.

B.3 Other Modulation Cases

As can be expected, other modulation schemes such as K-QAM with K>16 can also be addressed in a way similar to that in Sec. V. B1 or B2. With the appropriate modifications to the sign vector,

the correspoinding PAPR problem can be formulated as an unconstrained minimax optimization problem.

Remark 1: The proposed PAPR-redcution algorithm does not require transmission of any side information.

Remark 2: If a small amount of side information is manageable, the algorithm in [13] is a promising technique since it provides a considerate PAPR reduction without explicit side information. In such a system, the proposed algorithm can be smoothly integrated with the algorithm in [13] to achieve more PAPR reduction without any difficulties.

VI. Simulations

The proposed PAPR-reduction algorithms were applied to several multicarrier communication systems and the PAPR-reduction performance was evaluated and compared with that of the algorithms proposed in [15][17] for the baseband case and those in [13][17] for the passband case. A commonly used performance measure for PAPR-reduction algorithms is the clipping probability which is defined as the probability that the PAPR of the multicarrier signal exceeds a given PAPR threshold PAPR_0. Since high peaks of analog signal may occur after the D/A conversion [14], oversampling was applied to approximate the analog signal. In our simulations, all algorithms were applied using signals that were oversampled by a factor of 2, the sampling rate is then increased to 8 times the Nyquist sampling rate by a root-raised cosine filter with a rolloff factor of 0.12.

A. Baseband transmission system

The multicarrier communication system in our simulation had $N = 256$ subchannels where $n_u = 8$ subchannels (about 3% of the total subchannels) in the highest frequency range were

unused. In all active subchannels, QPSK modulation was assumed.

Example 1: The proposed algorithm described in Sec. IV.A was applied to reduce the PAPR of the transmit signal. Various values of n_a were used to obtain the peak-reduction vector $\mathbf{C}^*$, and the clipping probability versus various PAPR threshold values associated with vector $\mathbf{C}^*$ is plotted as the solid curves in Fig. 4. For the sake of comparison, the clipping probability obtained using the LP-based algorithm of Tellado in [15] and for the original multicarrier signal is plotted in the same figure as dashed and dot-dashed curves, respectively. It is evident that, after a small number of iterations, the proposed algorithm achieved significant performance improvement over that of the algorithm in [15]. For example, for a clipping probability of 10^{-3}, after 8 iterations the proposed PAPR-reduction algorithm with $n_a = 120$ offers a 0.88-dB improvement over the algorithm in [15].

The clipping probability obtained using the proposed PAPR-reduction algorithm was also compared with that obtained using the algorithm of Jones in [17] for various numbers of iterations, i.e., $itr = 5$, 10 and 100 and the target PAPR was set to be 9 dB. The results obtained are plotted in Fig. 5. For the sake of comparison, the clipping probability for the original multicarrier signals is also plotted as the dot-dashed curve. It can be observed that although the algorithm in [17] is capable of reducing the PAPR in a small number of iterations, a better performance was achieved using the proposed PAPR-reduction algorithm. For example, for a clipping probability of 10^{-3}, the proposed PAPR-reduction algorithm with $n_a = 120$ offers a 0.57-dB improvement over the algorithm in [17] with $itr = 10$.

The performance difference can be illustrated more explicitly using constellation-point patterns in the frequency domain as described below. The proposed PAPR-reduction algorithm with $n_a = 120$, $itr = 8$ and the algorithm in [17] with $itr = 100$ were applied to an arbitrarily chosen

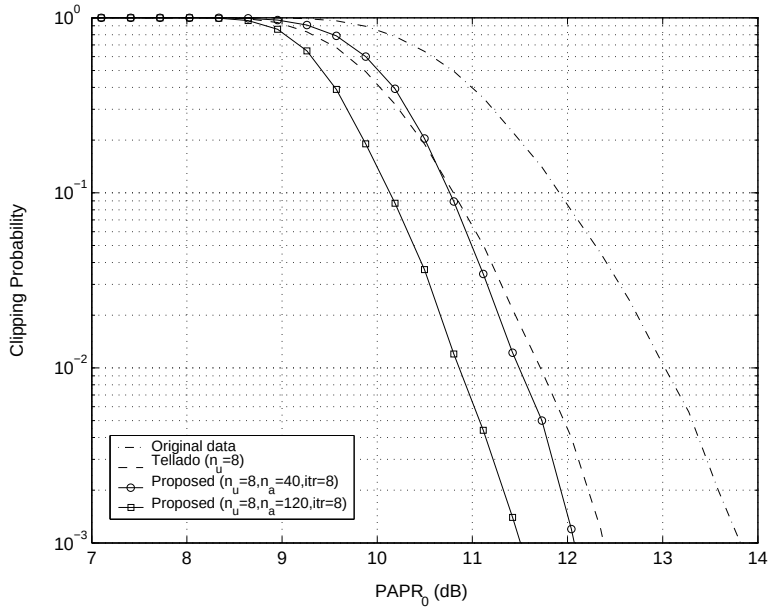

Fig. 4. Performance comparison of different PAPR-reduction algorithms.

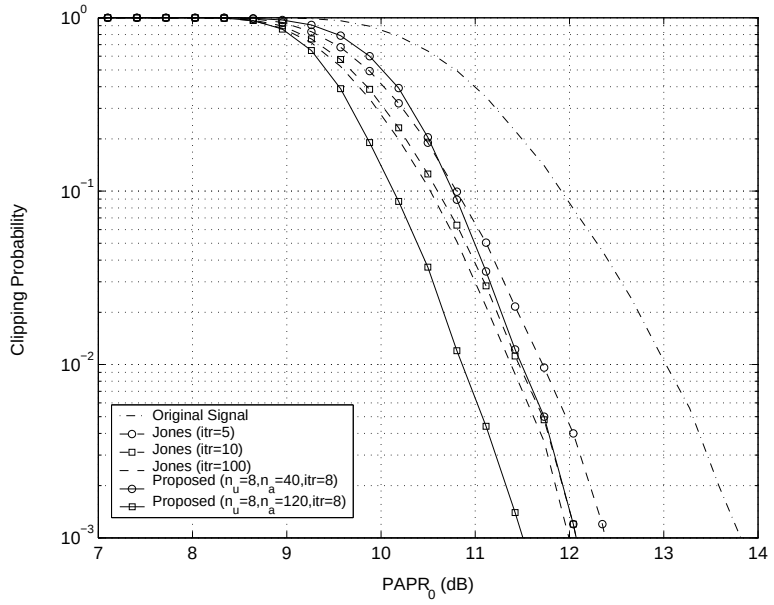

Fig. 5. Performance comparison of different PAPR-reduction algorithms.

multicarrier symbol $\mathbf{X}$ to obtain the corresponding peak-reduction vectors $\mathbf{C}^*$ and $\bar{\mathbf{C}}^*$, respectively. The constellation points obtained using the proposed algorithm in unused and active subchannels are shown in Fig. 6(a) and 6(b), respectively, and their counterparts obtained using the algorithm

in [17] are shown in Fig. 6(c) and 6(d), respectively. It is observed that the distributions of the optimal constellation points are considerablely different from their counterparts. Note that, as

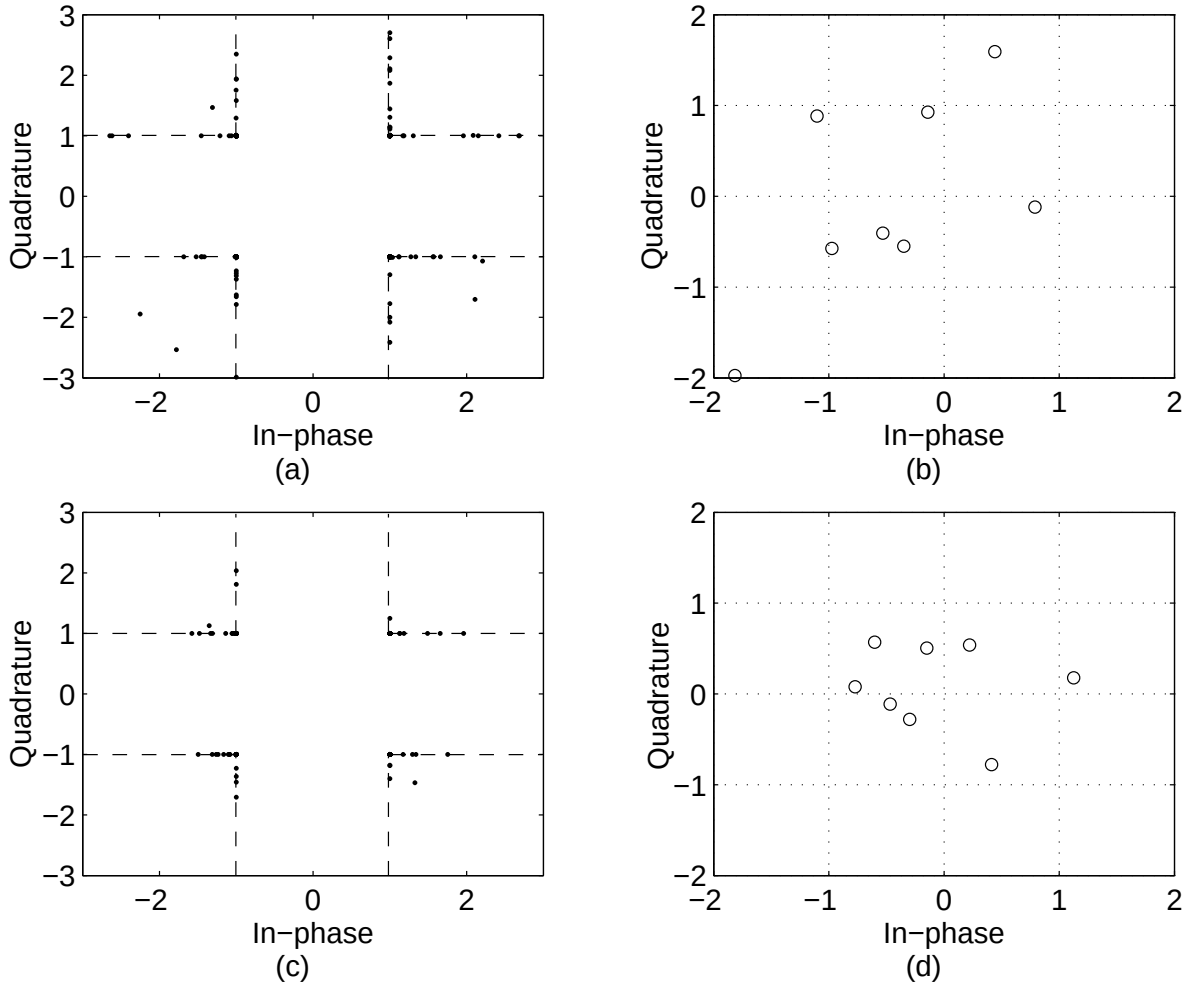

Fig. 6. Distributions of the modified constellation points using the proposed algorithm and the algorithm in [17]. (a) in unused subchannels by the proposed algorithm, (b) in active subchannels by the proposed algorithm, (c) in unused subchannels by the algorithm in [17], (d) in active subchannels by the algorithm in [17].

a result of superposition of the PAPR-reduction signal to the original signal, the signal power for this multicarrier symbol increases. However, in practice this will not be a problem as high peaks only show up with a small probability. Consequently, a PAPR-reduction algorithm need not to be applied all the time, thus the average power increase over a long duration is insignificant.

It is of interest to compare the computational complexity of the proposed algorithms with those of the existing algorithms [15][17]. The performance and complexity of the various PAPR reduction algorithms are given in Tables I and II, where the performance of each algorithm is quantified by its PAPR-reduction improvement in dB over the original data at the clipping probability of 10^{-3}. The complexity of each algorithm is indicated by the ratio of the CPU time for each algorithm to that of the proposed PAPR-reduction algorithm with $n_a = 120$, where the latter is set to unity.

TABLE I: Performance and Computational Complexity of various PAPR-Reduction Algorithms

PAPR-reduction algorithms	Proposed		Algorithm in [15]
	$n_a = 120,\ itr = 8$	$n_a = 40,\ itr = 8$	
Performance gain (dB)	2.34	1.78	1.46
Complexity	1	0.13	1.5

From Table I, the following conclusions can be drawn:

• Improved PAPR-reduction performance can be obtained by using the proposed algorithm. Meanwhile, the complexity of the proposed algorithm is lower than that of the algorithm in [15], i.e., for a clipping probability of 10^{-3}, the proposed algorithm with $n_a = 120$ improved the PAPR-reduction performance by 0.88 dB and required only two thirds of the computation complexity of that required by the algorithm in [15].

• The proposed PAPR-reduction algorithm offers a tradeoff between performance and computational complexity. Selecting fewer active subchannels for PAPR reduction can dramatically reduce the complexity of the proposed algorithm at the cost of moderate performance degradation. For example, by selecting $n_a = 40$ the amount of computation required by the proposed algorithm reduced to 8.7% of that required by the algorithm in [15], yet the PAPR-reduction improvement is still better than that of [15] by 0.32 dB.

TABLE II: Performance and Computational Complexity of various PAPR-Reduction Algorithms

PAPR-reduction algorithms	Algorithm in [17]			Proposed	
	$itr = 5$	$itr = 10$	$itr = 100$	$n_a = 40,\ itr = 8$	$n_a = 120,\ itr = 8$
Performance gain (dB)	1.47	1.78	1.82	1.78	2.34
Complexity	0.18	0.35	3.5	0.13	1

From Table II, it can be observed that:

• To achieve a similar performance, the computational complexity required by the proposed algorithm is much less than that required by the algorithm in [17]. For example, for a clipping probability of 10^{-3}, the proposed algorithm with $n_a = 40$ and the algorithm in [17] offer a similar performance, but the computational complexity of the former is only 40% of that of the latter.

• The PAPR-reduction performance of the algorithm in [17] reaches its limit after a certain number of iterations (in the present example, the algorithm in [17] does not offer significant performance gain after 100 iterations), but the proposed algorithm can still improve its performance by using more active subchannels for PAPR-reduction. Therefore, the proposed algorithm offers greater flexibility between performance and computational complexity, which is desirable if a large PAPR reduction with moderate computational compelxity increase is preferred.

B. Passband transmission systems

For passband multicarrier communication systems where all subchannels are active, the algorithms in [15] cannot be used but the algorithms in [13][17] and the proposed algorithm are applicable. The example presented below consists of two parts. In the first part, the algorithm proposed in Sec. V is simulated and compared with that of [17]. In the second part, under the assumption that the side information required by the method of [13] is available, it is demonstrated that the application of the proposed algorithm with the multicarrier signal selected by the method

of [13] as an initial point can reduce the PAPR by a substantial amount.

Example 2:

(a) We consider a multicarrier transmitter with $N = 64$ active subchannels. First, the proposed PAPR-reduction algorithm with various n_a was applied to obtain an optimal peak reduction vector $\mathbf{C}^*$, and the clipping probability is plotted as a solid curve in Fig. 7. Then, the performance of the algorithm in [17], with the target PAPR set to 6 dB, was evaluated and the clipping probability for various numbers of iterations, i.e., $itr = 20$ and 100 is plotted in the same figure as dashed curves. It is observed that performance improvement can be achieved by Jones' method with 20 iterations, but the algorithm's ability reaches its limit after 100 iterations. For example, for a clipping probability of 10^{-3}, 1-dB PAPR-reduction improvement can be achieved by Jones' method using 20 iterations, but only 1.2-dB improvement can be obtained by Jones' method using 100 iterations. On the other hand, for a clipping probability of 10^{-3}, the proposed algorithm with $n_a = 28$ and $itr = 4$ offers a 1-dB gain over the algorithm in [17] with $itr = 100$. For the comparison of computational complexity, as can be seen from the figure, the proposed PAPR-reduction algorithm with $n_a = 10$ and $itr = 4$ achieves a performance similar to that of Jones' method with 100 iterations. It turns out, however, that the amount of computation requied by the proposed method is 20% less than that required by Jones' method.

(b) We now consider a multicarrier transmitter with 64 active subcarrier where the side information required by method of [13] is available. The performance of the algorithm in [13] with the number of candidate sequences, $U = 4$ and 16, was evaluated and plotted in Figs. 8 and 9 as the dashed curves, respectively. In each case, the algorithm proposed in Sec. V with the best multicarrier signal selected by the method of [13] as an initial point was then applied. The PAPR-reduction performance achieved after 1 and 2 iterations is shown in the same figures as solid lines. For the

case of $U = 4$, the performance gain was 0.9 dB after 1 iteration and 1.5 dB after 2 iterations. For the case of $U = 16$, the performance gain was 0.2 dB after 1 iteration and 0.7 dB after 2 iterations.

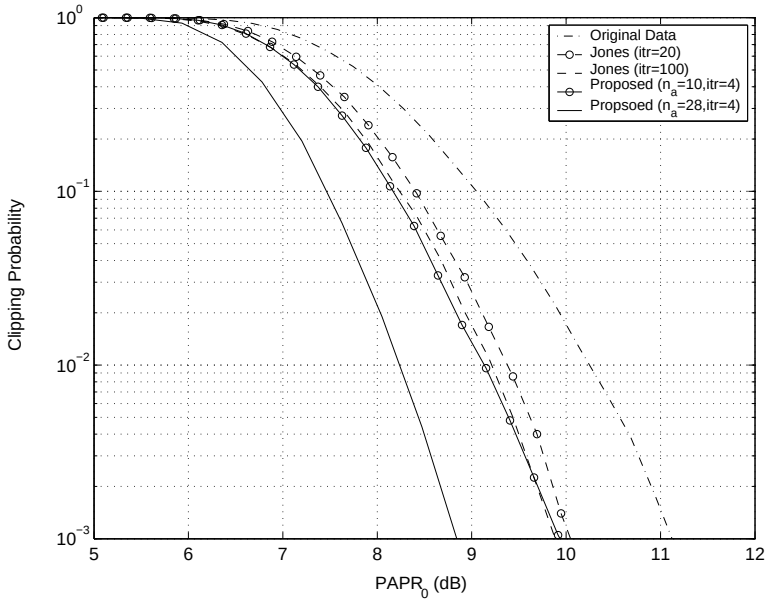

Fig. 7. Performance comparison of different PAPR-reduction algorithms.

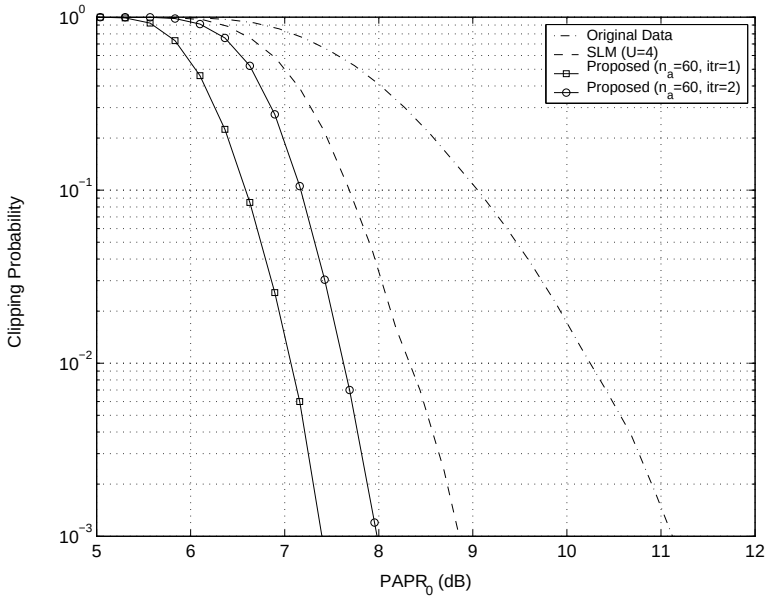

Fig. 8. Performance comparison of different PAPR-reduction algorithms.

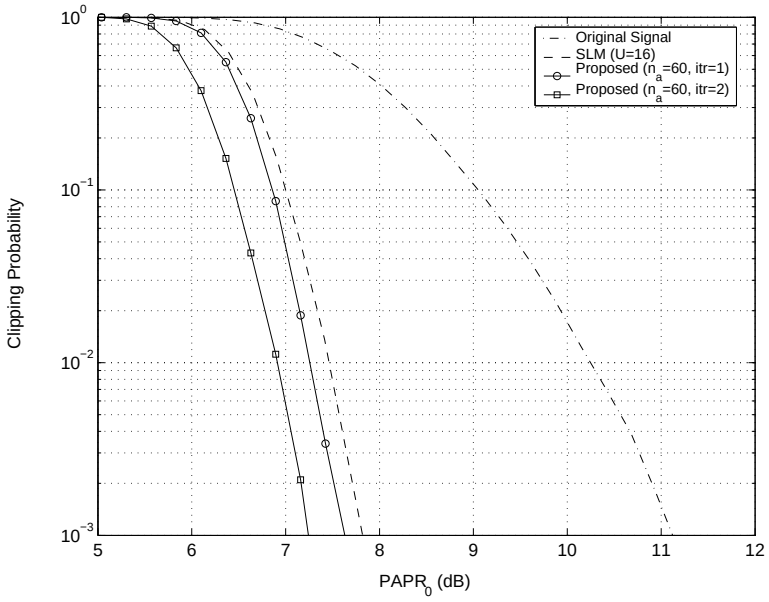

Fig. 9. Performance comparison of different PAPR-reduction algorithms.

VII. Conclusions

New PAPR-reduction algorithms for multicarrier commmunication systems that jointly optimize the constellation points in active subchannels and the unused subsymbols have been proposed. For baseband multicarrier systems, the proposed PAPR-reduction algorithm is based on an LP approach where all the subsymbols in unused subchannels and the exterior constellation points in active subchannels are optimized simultanneously. For passband multicarrier systems where all subchannels are active, a new PAPR-reduction algorithm has been proposed using an accelerated *least-pth* approach. Our simulations have demonstrated that, in many practical situations, considerable performance improvement can be achieved by the proposed PAPR-reduction algorithm over several existing algorithms and a tradeoff between performance and computational complexity is available.

References

[1] J. Bingham, "Multicarrier modulation for data transmission: an idea whose time has come," *IEEE Comm. Mag.*, pp. 5-14, May 1990.

[2] J. M. Cioffi, "A multicarrier primer," *ANSI document, T1E1.4 Technical Subcommittee,* no. 91-157, 1991.

[3] ETSI, "Radio broadcasting systems: digital audio broadcasting to mobile, portable and fixed receivers," European Telecommunication Standard, ETS 300-401, Feb. 1995.

[4] ETSI, "Digital video broadcasting: framing structure, channel coding, and modulation for digital terrestrial television," European Telecommunication Standard, ETS 300-744, Aug. 1997.

[5] R. V. Nee and R. Prasad, *OFDM for Wireless Multimedia Communications*, Artech House Publisher, 2000.

[6] W. Liu, J. Lau and R. S. Cheng, "Considerations on applying OFDM in a highly efficient power amplifier," *IEEE Trans. Circuits Syst. II*, vol. 46, pp. 1329-1336, Nov. 1999.

[7] D. J. G. Mestdagh, P. Spruyt, and B. Biran, "Analysis of clipping effect in DMT-based ADSL systems," *Proc. of IEEE International Conference on Communications*, pp. 293-300, 1994.

[8] X. Li and L. J. Cimini, Jr., "Effects of clipping and filtering on the performance of OFDM," *IEEE Communications Letters*, pp. 131-133, May 1998.

[9] A. E. Jones and T. A. Wilkinson, "Combined coding for error control and increased robustness to system nonlinearities in OFDM," *Proc. of IEEE 46th Vehicular Technology Conference*, pp. 904-908, May 1996.

[10] R. D. J. Van Nee, "OFDM codes for peak-to-average power reduction and error correction," *Proc. of IEEE Global Telecommunications Conference*, pp. 740-744, Nov. 1996.

[11] J. A. Davis and J. Jedwab, "Peak-to-mean power control and error correction for OFDM transmission using Golay sequences and Reed-Muller codes," *Electronics Letters*, pp. 740-744, Nov. 1996.

[12] S. Mueller, R. Baeuml, R. Fischer, and J. Huber, "OFDM with reduced peak-to-average power ratio by multiple signal representation," *Annals of Telecommunications,* Feb. 1997.

[13] M. Breiling, S. Mueller-Weinfurtner, and J. Huber, "Distortionless reduction of peak power without explicit side information," *Proc. of IEEE Global Telecommunications Conference*, pp. 1494-1498, 2000.

[14] C. Tellambura, "Phase optimization criterion for reducing peak-to-average power ratio for OFDM," *Electronics Letters,* pp. 169-170, Jan. 1998.

[15] J. Tellado and J. M. Cioffi, "PAR Reduction in multicarrier transmission systems," *ANSI document, T1E1.4*

Technical Subcommittee, contribution number 97-367, Dec. 1997.

[16] J. Tellado, *Peak to Average Power Ratio Reduction for Multicarrier Modulation*, Ph.D. Dissertation, Stanford University, Sep. 1998.

[17] D. Jones, "Peak power reduction in OFDM and DMT via active channel modification," *Proc. of 33rd Asilomar Conference on Signals, Systems and Computers*, pp. 1076-1079, 1999.

[18] C. Charalambous, "Acceleration of the least pth algorithm for minimax optimization with engineering applications," *Math. Programming,* vol. 17, pp. 270-297, 1979.

[19] B. S. Krongold, *New Techniques for Multicarrier Communications Systems*, Ph.D. Dissertation, University of Illinois at Urbana-Champaign, Dec. 2001.

[20] B. S. Krongold and D. Jones, "A new tone reservation method for complex-baseband PAR reduction in OFDM systems," *Proc. of ICASSP 2002*, pp. 2321-2324, 2002.

[21] O. L. Mangasarian, *A Newton Method for Linear Programming*, Data Mining Institute Technical Report 02-02, University of Wisconsin, Mar. 2002.